Current Science
CS 5 (3), 2619-2631 (2025)
Received 26 Feb 2025 | **Revised 25 March** 2025 | **Accepted 23 April**. 2025 | **Online Available 27 May** 2025
https://doi.org/ 10.52845/CS/2025-5-3-45

Current Science
Current Science

OPEN ACCESS **ISSN(O)2795-8639**

Original Article

Machine Learning Molecular Dynamics Simulations on Diffusion of SF_6 and N_2 in SF_6/N_2 Mixtures

Ke Zhao[1]*, Hanyan Xiao[1], Tianxin Zhuang[1], Jinggang Yang[1], Ze Yin[1], Zhaohui Zhang[1]

[1]Jiangsu Electric Power Company Research Institute, Nanjing 211103, P.R. China

***Corresponding Author: Ke Zhao**

Abstract:
Sulfur hexafluoride (SF_6) is widely used for an insulating and arc extinguishing medium in high voltage electrical equipment due to its excellent dielectric properties and insulation performances. However, SF_6 is a potent greenhouse gas, leading to a significant influence on the environment by the large use of SF_6. SF_6 mixed with inert gas such as N_2 is a more promising way to reduce the use of SF_6. The diffusion properties of SF_6/N_2 mixtures play a crucial role in the gaseous mixture separation or replenishment, determining the proportion and uniformity of the mixtures. Combining ab initio molecular dynamics (AIMD) and machine-learning molecular dynamics (MLMD) simulations of SF_6 and N_2 dynamics in SF_6/N_2 mixtures, we systematically illustrate the anomalous characteristics of both SF_6 and N_2 motion. At short times, both SF_6 and N_2 performs super-diffusion through the ballistic motion. At intermediate times, a combination of the SF_6 molecular flexibility and cage effect result in the larger plateau value, while N_2 molecular showed no plateau stage. At longer times, both SF_6 and N_2 gradually turns to normal diffusion. A theoretical model is also offered to quantitatively describe this abnormal diffusion. This work gives a more completely physical understanding of SF_6 and N_2 dynamics in SF_6/N_2 mixtures, which provides important references for SF_6 /N_2 mixed electrical equipment leakage supplement.

Keywords: Diffusion; Mixtures; Machine-learning molecular dynamics; Anomalous diffusion; Theoretical model

Introduction

Sulfur hexafluoride (SF_6) is widely used for an insulating and arc extinguishing medium in high voltage electrical equipment due to its excellent dielectric properties and insulation performances.[1,2] However, SF_6 is a potent greenhouse gas with high global warming potential value and long atmospheric lifetime, leading to a significant influence on the environment by the large use of SF_6, therefore, the study on alternative gases has received extensive attention.[3] SF_6 mixed with inert gas such as N_2 is a more promising way to reduce the use of SF_6. SF_6/N_2 mixed gases are cheaper than pure SF_6 and, under the suitable conditions of pressure, can achieve equally well for both arc interruption and electrical insulation.[1] Currently, some power grids use SF_6 /N_2 mixed gas in areas with lower temperatures.[4] The equipment will inevitably have slow leakage defects during operation, and gas replenishment is inevitable. In order to ensure the proportion and uniformity of the mixed gas, the diffusion characteristics of the mixed gas need to be understood.[4] Another important issue related to the use of these mixed gases is the SF_6 recovery. The separation of SF_6/N_2 mixed gases have been reported and experimentally tested with different methods, most of them using adsorbents.[5]

The performance of the above-mentioned processes is related to the operating conditions at macroscopic scale and the different phenomena taking place at the microscopic level.[6] The design and optimization of these processes needs to know the underlying physical properties of the mixture to be replenished or separated, such as the shear viscosity and diffusion coefficient. In order to obtain these transport properties, theoretical

methods are widely used to describe transport coefficients in binary gaseous mixtures, and several empirical models are proposed in the literature.[7,8] The viscosities of two SF_6/N_2 mixed gases with N_2 mole fractions of 0.3357 and 0.8780 are measured and reported at atmospheric pressure in a temperature range from 298 to 483 K.[9] The binary diffusion coefficients are derived from the viscosity data by using the Chapman-Enskog method of solution of the Boltzmann equation. In addition, the viscosity and the diffusion coefficients for SF_6/N_2 mixed gas with equimolar fraction are obtained by using a similar approach at atmospheric pressure but in a wider temperature range from 273 to 1273 K.[10]

From a theoretical point of view, even if SF_6 and N_2 have been successfully modeled as spherical molecules in some applications, it is reported that the SF_6 molecular flexibility plays an important role in some of its properties.[11] Since SF_6 and N_2 have different molecular sizes, the deviations from ideality for specific properties may arise from this molecular flexibility. Some efforts have been made to find the relationship of the macroscopic behavior of SF_6 and its microscopic behavior from a molecular perspective.[12–14] The behavior of binary mixtures using both simple Lennard-Jones potentials[15–20] and anisotropic models for complex and/or polar molecules.[21–26] are explored by using molecular dynamics (MD) simulations. The bulk transport properties (diffusion coefficients and shear viscosities) of SF_6/N_2 mixtures with different compositions at 300 K and 1 MPa are investigated by a series of MD simulations. Composition dependences of both diffusion coefficients and shear viscosities are found by MD simulations with anisotropic force fields, which differs from the predictions with the simpler Lennard-Jones potentials. Unfortunately, more insights into the dynamics of SF_6/N_2 mixtures with different compositions in a long-time range have not yet been advanced. In particular, the relevance of the SF_6 molecular flexibility to diffusion coefficients of SF_6/N_2 mixtures has to be addressed. Thus, the dynamics of isolated SF_6 in SF_6/N_2 mixtures is needed to be fully characterized. Detailed theoretical model for the dynamics of SF_6 diffusion is also needed to understand the SF_6/N_2 mixtures diffusion behavior.[11]

The abovementioned force field for the SF_6 and N_2 molecule uses the predefined mathematical form such as LJ potential quantifying the interatomic interactions, but this approximation tends to oversimplify the physical nature of interatomic interactions. Therefore, it is necessary to develop a potential with accuracy and efficiency to simulate the dynamics of SF_6/N_2 mixtures. The Machine Learning (ML) potential is a good option. ML potentials are one of the most representative applications of machine learning methods[27–30], which use DFT results as a dataset and train mappings between atomic structures and potential energy based on purely mathematical structures such as neural networks or Gaussian processes[31]. In this way, ML potentials successfully bridge DFT and MD, achieving potential surfaces with DFT accuracy while maintaining the efficiency of MD simulations, offering the possibility of solving the dilemma of accuracy and efficiency. In addition, the material systems and application environments do not limit the application of ML potentials. It can be applied to different types of material systems such as metals[32,33], calcium titanate[34] and semiconductors[35–38], as well as to complex atomic environments at high temperatures[39], high pressures[40] and irradiation[41,42].

In this paper, we constructed a database using DFT calculations and developed ML potential with DFT accuracy to describe the dynamics of SF_6/N_2 mixtures. Based on the obtained model, we first calculated the structural properties of SF_6 and N_2 to verify the accuracy of the ML potential. Then, results of our MD simulation on the dynamics of SF_6/N_2 mixtures are shown, discussing the diffusion process of the SF_6/N_2 mixtures in detail, illustrating the anomalous characteristics of the SF_6 motion in SF_6/N_2 mixtures. Finally, we developed a theoretical model, and analyzing the abnormal SF_6 diffusion behavior during the diffusion process.

2 Machine Learning Potential

2.1 Database

To construct a ML model that can capture describe the dynamics of SF_6/N_2 mixtures, a dataset related to the SF_6/N_2 mixtures was built. The data set consists of both pure and mixed gases. In the case of mixed gases, different mixing ratios of SF_6 and N_2 were considered. All

configurations come from either *ab initio* MD (AIMD) simulations. The details are shown in **Table 1** below. The type and number of configurations are based on physical intuition and past practice. The dataset contains a total of 159,000 configurations.

Table 1 Summary of the database for the dynamics of SF_6/N_2 mixtures. The first column shows the corresponding properties of the configurations. The second column shows the type of configurations. The third column shows the number of atoms of the configurations. The fourth column shows the number of configurations. The last column shows the number of atomic environments, which is equal to the number of atoms times the number of configurations.

Corresponding properties	Structure type	No. atoms	No. configurations	No. atomic environments
Pure gas	Single N_2 molecule	2	12000	24000
	Single SF_6 molecule	6	12000	72000
	N_2 molecules	116	9000	1044000
		252	9000	2268000
	SF_6 molecules	84	9000	756000
		168	9000	1512000
Gas mixture	$N(SF_6)$: $N(N_2)$ = 1: 26	236	9000	2124000
	$N(SF_6)$: $N(N_2)$ = 2: 47	108	9000	972000
	$N(SF_6)$: $N(N_2)$ = 2: 21	224	9000	2016000
	$N(SF_6)$: $N(N_2)$ = 4: 37	102	9000	918000
	$N(SF_6)$: $N(N_2)$ = 6: 31	208	9000	1872000
	$N(SF_6)$: $N(N_2)$ = 2: 9	96	9000	864000
	$N(SF_6)$: $N(N_2)$ = 8: 21	196	9000	1764000
	$N(SF_6)$: $N(N_2)$ = 1: 2	88	9000	792000
	$N(SF_6)$: $N(N_2)$ = 1: 1	180	9000	1620000
	$N(SF_6)$: $N(N_2)$ = 5: 3	82	9000	738000
	$N(SF_6)$: $N(N_2)$ = 11: 5	174	9000	1566000
	$N(SF_6)$: $N(N_2)$ = 23: 5	171	9000	1539000

The Vienna *Ab initio* simulation package (VASP) was used for DFT computations[43–45]. The enhanced projection wave method[46] and the PBE generalization function[47] were used. The truncation energy of the plane wave basis was set to 500 eV. In the AIMD simulations, the NVT ensemble was used, the time step was set to 0.5 fs, and the temperature was controlled by employing the Nosé-Hoover thermostat. 2×2×2 Monkhorst-Pack k-points mesh was used in AIMD simulations. DFT calculated the potential energy of each configuration and the force per atom in the dataset, which will be the dataset for supervised machine learning training.

2.2 Model Training

Based on the above data set, we trained a ML potential using DeePMD[27] artificial neural network architecture. Atoms within a cutoff radius of 6 Å were taken into account for the local atomic environment of the ML potential. The batch size was set to 4 and the training ran through 10^6 batches. The starting and ending learning rate was set to 5×10^{-3} and 5×10^{-8}, respectively and the learning rate was exponentially decayed during the training. Finally, a deep neural network of three hidden layers with 240, 240, and 240 nodes was employed to map the local atomic environment to the atomic energy contributions.

Comparisons between the database and ML results on energies and forces are shown in **Figure 1**. The resulting root mean squared errors (RMSE) of the energies are 8.50 and 8.49 MeV/atom for training and test sets, respectively. As for forces, the RMSE are 50.76 and 50.90 MeV/Angstrom for training and test sets, respectively. The RMSE values of the ML potential are consistent with the typical RMSE values for ML models[47].

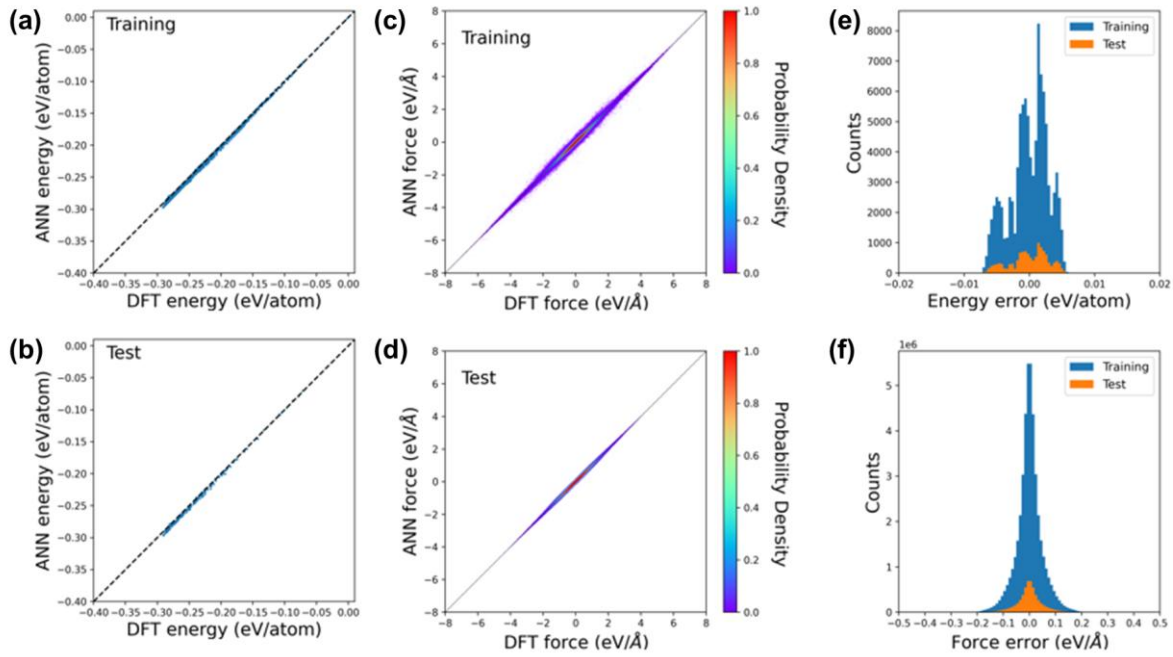

Figure 1 Comparisons of the ML results with respect to the references DFT data. (a) and (b) show the comparisons of energies per atom for the training and test set, respectively. (c) and (d) exhibit force comparisons for the training and test set. 2D histogram plots are used to show the density distribution of errors. (e) and (f) display the error distributions for energies and forces for training and test set.

After obtaining the ML potential, we computed the molecular structure parameters for N_2 and SF_6. These computations were subsequently compared with DFT results to ensure the accuracy of the ML potential. The specific values from these computations are documented in **Table 2**. It is evident from Table 1 that the molecular structure parameter calculations for both N_2 and SF_6 using the ML potential align with the DFT reference values, which means that the developed ML potentials can reliably characterize the molecular geometry of N_2 and SF_6.

Table 2 Comparison of geometric parameters of N_2 and SF_6 based on ML potential and DFT

Molecular name	Bond length (Å)/Bond angle (deg)	DFT	ML
N_2	N_1-N_2	1.111	1.111
SF_6	S_1-F_2	1.587	1.586
	F_2-S_1-F_3	90.0	90.0
	F_2-S_1-F_4	180.0	180.0

3 Result and Discussion

The power-law formulation of the mean-square displacement (MSD) over time is used to characterize the dynamical properties of particle transport[48],

$$\langle|\vec{r}(t)-\vec{r}(0)|^2\rangle \simeq K_\alpha t^\alpha \quad (1)$$

here $\vec{r}(t)$ is a position of particle at time t, brackets $\langle ... \rangle$ stands for the ensemble average, and α is used to differentiate the diffusion behavior (α <1, α =1, and α >1 represents the sub-diffusion, normal diffusion, and super-diffusion, respectively).

Because of a limited number of particle transport trajectories, the time-averaged mean-square displacement (TAMSD) as a function of the lag time are alternatively calculated in terms of the time series $r(t)$[48], generally characterized by

$$\overline{\delta^2(\Delta,T)} = \frac{1}{T-\Delta}\int_0^{T-\Delta}|\vec{r}(t+\Delta)-\vec{r}(t)|^2 dt \qquad (2)$$

where T and Δ are the total measurement time and the lag time, respectively. On the basis of the individual TAMSDs, the corresponding average over the group of N trajectories can be obtained by[49],

$$\langle\overline{\delta^2(\Delta)}\rangle = \frac{1}{N}\sum_{i=1}^{N}\overline{\delta_i^2(\Delta)} \quad (3)$$

To investigate SF_6 and N_2 dynamics in SF_6/N_2 mixtures, we performed MLMD calculations by using the NVT ensemble (constant number of particles, volume, and temperature) with a time step width of 0.5 fs. The temperature was maintained at 300 K where the Nosé-Hoover thermostat was adopted[50,51]. Prior to initiating the formal simulation, the structure undergoes an initial relaxation at 300 K for a duration of 5 ps within the NPT ensemble. Throughout this relaxation phase, the pressure is maintained at 0.6 MPa, aligning with the pressure of the gas present in the Gas insulated switchgear (GIS). After structure relaxation, we continued to calculate the system for another 2ns to obtain the trajectory of SF_6 and N_2 diffusion. The TAMSDs calculations for pure N_2, pure SF_6, and an SF_6/N_2 mixtures ($N(SF_6)$: $N(N_2)$ = 1:1) were conducted and the results are shown in **Figure 2.**

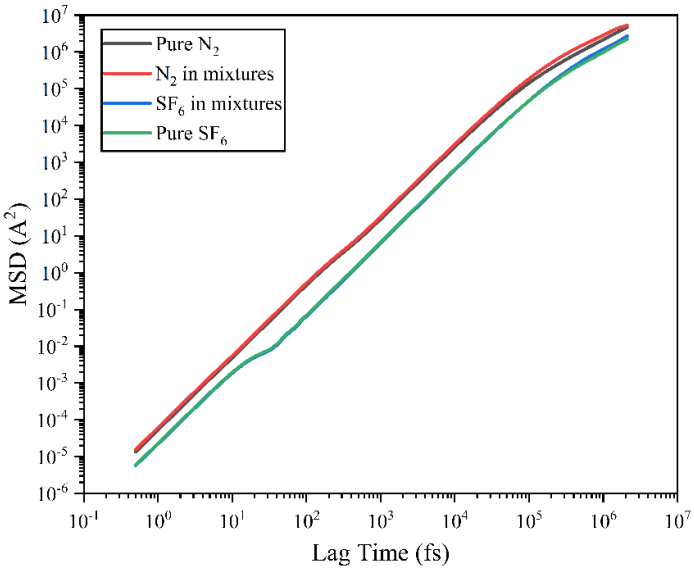

Figure 2 Time-averaged MSDs of gas for 2ns trajectory.

As illustrated in **Figure 2.**, the diffusion of N_2 in pure gas or mixture can be divided into two stages:

- from zero to about 300 ps, the N_2 undergoes a super diffusive, of which around 100 ps to 300 ps represents a transition from super diffusive to normal diffusion. During this transition, the power exponent gradually diminishes from values greater than 1 to eventually equal 1, indicative of normal diffusion;
- for longer times after 300ps, N_2 exhibits normal diffusion characteristics.

Unlike N_2, although the diffusion trend of SF_6 in its pure form and in mixtures remain consistent, the diffusion of SF_6 can be divided into four stages:

- in the initial 15fs (from zero to about 15fs), the power exponent of SF_6 diffusion is greater than 1, and the diffusion form exhibits super diffusive;
- after 20fs, which is roughly between 15fs to 35fs, there is a noticeable deceleration in the acceleration of TAMSD;
- within the intermediate-length timeframe of 35 fs to 500 ps, the diffusion form of SF_6

returns to super diffusive again, and the transition from super-diffusion to standard diffusion is concluded at approximately 400 ps, spanning from roughly 100 ps to 500 ps.

- at longer times (from about 500ps to about 2ns), the SF_6 diffusion returns back to the normal diffusion regime.

Furthermore, the diffusion coefficients of N_2 and SF_6 in the SF_6/N_2 mixture, obtained through data fitting of the normal diffusion stage, are 0.01543 cm^2/s for N_2 and 0.01822 cm^2/s for SF_6. Among them, the diffusion coefficient of SF_6 aligns closely with the findings of Suzuki's research[52].

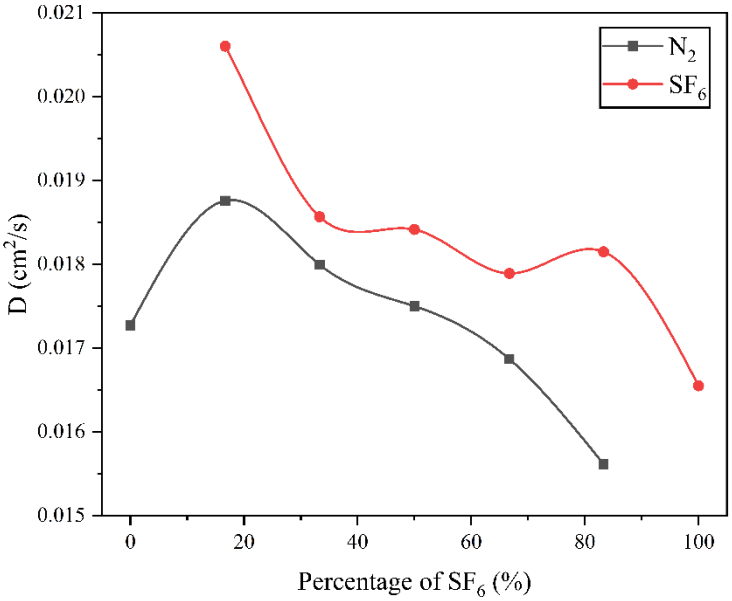

Figure 3 Comparison of the effect of SF_6 concentration in the mixtures on the diffusion coefficients of N_2 and SF_6, concentration 0 means pure N_2 and concentration 100 means pure SF_6.

In SF_6/N_2 mixtures, the ratio between the two gases is variable, necessitating an investigation into the impact of SF_6 concentration on the diffusion coefficients of both SF_6 and N_2. Utilizing the ML potential, the diffusion coefficients of N_2 and SF_6 of SF_6/N_2 mixtures with different SF_6 concentrations were simulated. The simulation methodology was consistent with the previous paper, and the derived results are presented in **Figure 3.**

Figure 3 illustrates the diffusion coefficients of N_2 and SF_6 in mixtures, plotted against the concentration of SF_6. As the SF_6 concentration increases, the diffusion coefficients of N_2 and SF_6 exhibit distinct trends. For N_2, the diffusion coefficient increases first and then decreases with the increase of the concentration of SF_6 in mixtures, and the diffusion coefficient is lower than that of pure N_2 when the SF_6 concentration surpasses 66.7%. Different from N_2, the diffusion coefficient of SF_6 decreases with the increase of the concentration of SF_6 in mixtures, and the diffusion coefficients of SF_6 in all mixtures are higher than that of pure SF_6.

To study in depth the anomalous diffusion of SF_6 and N_2 in SF_6/N_2 Mixtures, vibrational motions of the SF_6 and N_2 are explored. According to a Fourier transform of the atomic velocity autocorrelation function (VACF) of both SF_6 and N_2, the normalized vibrational density of states (VDOS) are calculated as shown in **Figure 4**. We can observe that there are seven peaks in the DOS of the normal region: six are located below 50 THz (low-frequency peaks), and one is around 110 THz (a high-frequency peak corresponding to the N–N stretching modes). High-frequency vibrations are typically associated with bond stretching modes, while low-frequency peaks correspond to bond bending or wagging motions[53,54]. In SF_6, taking one F atom as a reference, four other F atoms are symmetrically spaced around it, and one F atom is located at a relatively longer distance. Among the six peaks associated with the F atoms, two have frequencies that match those of the S atom. The lower one

corresponds to the bending modes of the S–F bond, and the higher one to its stretching modes. The remaining four peaks of the F atom represent two types of F–F bond vibrations—stretching and bending frequencies. It is worth noting that the S–F bending frequency at 25 THz corresponds well to the MSD inflection point at around 40 fs during the transition from short to intermediate timescales, as shown in **Figure 2**.

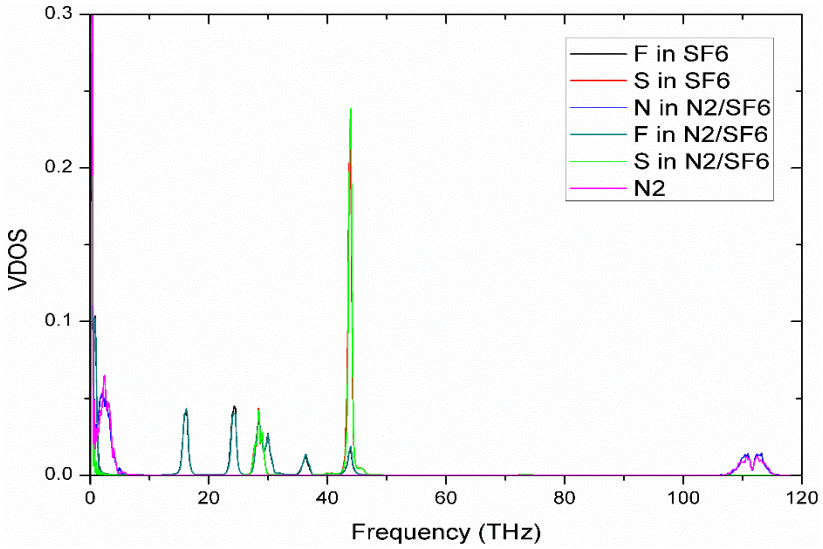

Figure 4 Power spectra of translational VACF.

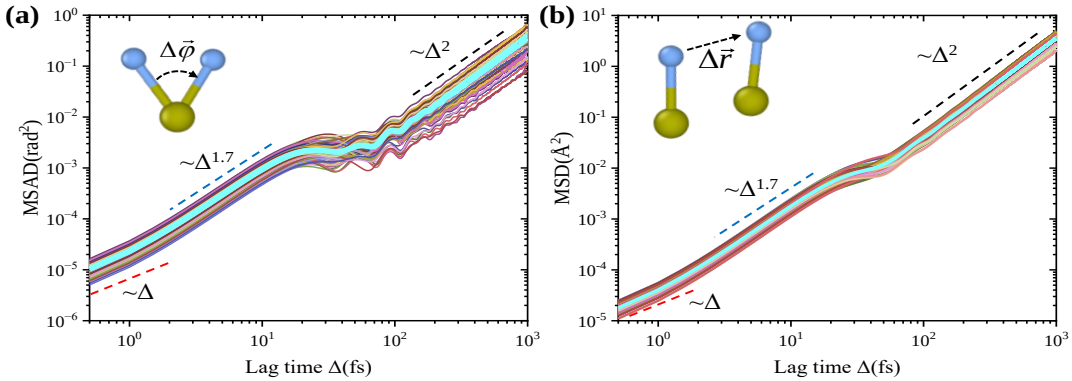

Figure 5 Time-averaged MSAD for SF bond rotation. The cyan line represents the average data of all curves. (b) Time-averaged MSD for F atom movement. The cyan line represents the average data of all curves.

The angular motion of the SF bond was analyzed because the rotation of the SF bond plays a crucial role in proton motion, especially in a short - term period. As depicted in **Figure 5a**, the time - averaged mean - square angular displacement (MSAD) of the SF bond rotation during the diffusion of SF_6 was calculated,

$$\overline{\delta^2(\Delta, \mathrm{T})} = \frac{1}{T-\Delta}\int_0^{T-\Delta} |\vec{\varphi}(t+\Delta) - \vec{\varphi}(t)|^2 dt$$

Here, Δ and T represent the lag time and the total measurement time respectively, and $\vec{j}(t)$ denotes the total angular displacement of the SF bond[55]. Although the MSAD values vary among different F atoms, thanks to the large sample size, the averaged data (represented by the cyan line in **Figure 5a** demonstrates the characteristics of normal rotation with a slope close to 1 in a shorter time frame and hyper - rotation with a slope of approximately 1.7 in a longer time frame. Moreover, after a relatively long period of sub-rotation, it transforms into a hyper - rotation characteristic with a slope of about 2. In addition, **Figure 5b** shows the calculation of the mean square displacement (MSD) associated with the displacement of F atoms in **Figure 5a**. Its variation trend is consistent with the curve in **Figure 2** and covers the plateau period in **Figure**

2. The change in the slope of its curve is consistent with the rotation of the S - F bond in **Figure 5a**, indicating that the plateau period in **Figure 2** is caused by the rotation of the S - F bond in the SF_6 molecule.

To provide a generalized explanation of the anomalous dynamics, an analytical model incorporating the two aforementioned fractional Brownian motions (FBMs) is proposed, based on the modified Richard expression[56], which is used to characterize the diffusion process in terms of short-time super-diffusion, medium-time super-diffusion, and long-time normal-diffusion.

$$MSD(\Delta) = \frac{K_s \Delta^{\varepsilon_s}}{\left[1+\left|\frac{K_s \Delta^{\varepsilon_s}}{\xi_s}\right|^{\theta_m}\right]^{1/\theta_m}} + \frac{(K_s+K_m)\Delta^{\varepsilon_m}}{\left[1+\left|\frac{(K_s+K_m)\Delta^{\varepsilon_m}}{\xi_m}\right|^{\theta_l}\right]^{1/\theta_l}} + K_l\Delta \quad (4)$$

where the relevant parameters are defined as follows:

- $K_s = K_{s\tau} + (K_{s0} - K_{s\tau})\tau_1$ (5a)
- $\xi_s = \xi_{s\tau} + (\xi_{s0} - \xi_{s\tau})\tau_1$ (5b)
- $\theta_s = \theta_{s\tau} + (\theta_{s0} - \theta_{s\tau})\tau_1$ (5c)
- $K_m = K_{m\tau} + (K_{m0} - K_{m\tau})\tau_1$ (5d)
- $\xi_m = \xi_{m\tau} + (\xi_{m0} - \xi_{m\tau})\tau_2$ (5e)
- $\theta_m = \theta_{m\tau} + (\theta_{m0} - \theta_{m\tau})\tau_2$ (5f)
- $K_l = K_{l\tau} + (K_{l0} - K_{l\tau})\tau_2$ (5g)

where parameters $K_{s\tau}$, K_{s0}, $\xi_{s\tau}$, ξ_{s0}, $\theta_{s\tau}$, θ_{s0} are defined for the short-time diffusion, $K_{m\tau}$, K_{m0}, $\xi_{m\tau}$, ξ_{m0}, $\theta_{m\tau}$, θ_{m0} are defined for the medium-time diffusion, $K_{l\tau}$, K_{l0} are defined for long-time diffusion. In particular, $\xi_{s\tau}$ and $\xi_{m\tau}$ accounts for the MSD near the transition from short-time super-diffusion to the medium-time super-diffusion and medium-time super-diffusion to long-time normal diffusion, $K_{s\tau}$ and ε_s correspond the diffusion parameters for short-time super-diffusion, $K_{m\tau}$ and ε_m correspond the diffusion parameters for medium-time super-diffusion and $K_{l\tau}$ corresponds the diffusion parameters for long-time normal diffusion. The parameter τ_1 and τ_2 describes the transition from short-time super-diffusion to the medium-time super-diffusion and medium-time super-diffusion to long-time normal diffusion are given by:

$$\tau_1 = \left[\frac{\Delta^{t_{11}}}{\Delta^{t_{11}} + T_1^{t_{11}}}\right]^{t_{21}} \quad (6a)$$

$$\tau_2 = \left[\frac{\Delta^{t_{12}}}{\Delta^{t_{12}} + T_2^{t_{12}}}\right]^{t_{22}} \quad (6b)$$

where T_1 and T_2 accounts for the lag time near the transition from short-time super-diffusion to the medium-time super-diffusion and medium-time super-diffusion to long-time normal diffusion. All parameters of this theoretical model are listed in **Table 3.**

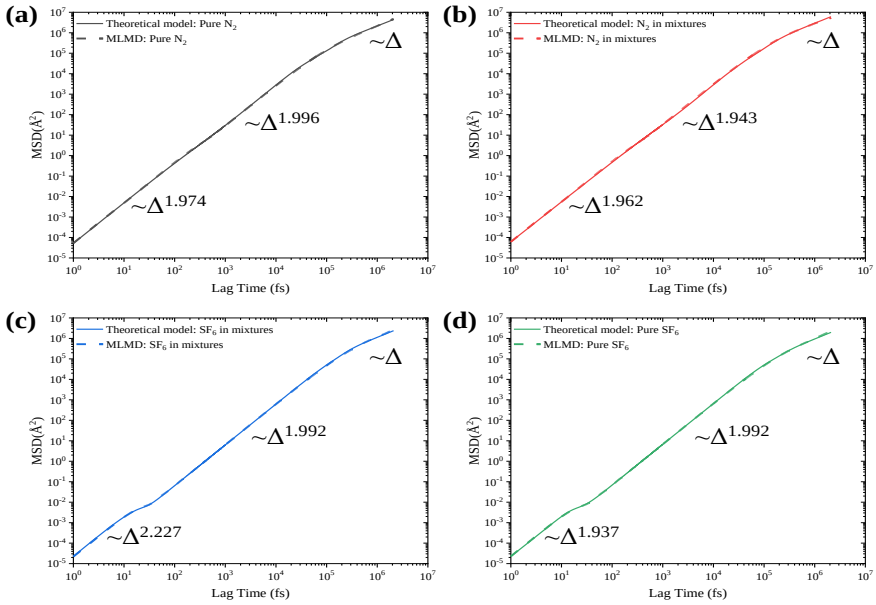

Figure 6 Fit of the Pure N_2 (a), N_2 in mixtures (b), SF_6 in mixtures (c) and Pure SF_6 (d).

Table 3 Parameters for modified Richard MSD model.

Parameter	Pure N_2	N_2 in mixtures	SF_6 in mixtures	Pure SF_6
$K_{s\tau}$	2.608×10^{-5}	3.079×10^{-5}	1.228×10^{-5}	1.122×10^{-5}
K_{s0}	0.000×10^{0}	0.000×10^{0}	0.000×10^{0}	0.000×10^{0}
$K_{m\tau}$	0.000×10^{0}	0.000×10^{0}	0.000×10^{0}	0.000×10^{0}
K_{m0}	2.987×10^{-5}	6.028×10^{-5}	6.659×10^{-6}	7.100×10^{-6}
$K_{l\tau}$	0.000×10^{0}	0.000×10^{0}	0.000×10^{0}	0.000×10^{0}
K_{l0}	2.067×10^{0}	2.879×10^{0}	1.132×10^{0}	9.404×10^{-1}
$\xi_{s\tau}$	2.000×10^{2}	2.000×10^{2}	2.000×10^{1}	1.400×10^{1}
ξ_{s0}	1.000×10^{2}	1.000×10^{1}	2.000×10^{1}	2.000×10^{0}
$\xi_{m\tau}$	8.500×10^{4}	5.000×10^{4}	1.250×10^{5}	1.250×10^{5}
ξ_{m0}	1.000×10^{5}	8.000×10^{4}	1.000×10^{3}	1.000×10^{3}
$\theta_{s\tau}$	3.600×10^{-1}	4.600×10^{-1}	2.000×10^{0}	2.000×10^{0}
θ_{s0}	1.800×10^{-1}	1.800×10^{-1}	4.000×10^{0}	4.000×10^{0}
$\theta_{m\tau}$	1.200×10^{0}	1.200×10^{0}	1.000×10^{0}	1.000×10^{0}
θ_{m0}	8.000×10^{0}	6.000×10^{0}	8.000×10^{-1}	8.000×10^{-1}
ε_s	1.974×10^{0}	1.962×10^{0}	2.227×10^{0}	1.937×10^{0}
ε_m	1.996×10^{0}	1.943×10^{0}	1.992×10^{0}	1.992×10^{0}
T_1	5.000×10^{1}	2.500×10^{2}	2.600×10^{1}	1.780×10^{1}
T_2	1.000×10^{5}	1.000×10^{5}	2.250×10^{5}	2.250×10^{5}
t_{11}	6.000×10^{-1}	6.000×10^{-1}	5.500×10^{0}	3.800×10^{0}
t_{12}	2.400×10^{0}	2.000×10^{0}	3.500×10^{0}	3.500×10^{0}
t_{21}	5.000×10^{0}	5.000×10^{0}	1.200×10^{-1}	1.200×10^{0}
t_{22}	2.200×10^{0}	1.400×10^{0}	8.000×10^{-1}	8.000×10^{-1}

The results of fitting the pure N_2, N_2 in mixtures, SF_6 in mixtures and Pure SF_6 curves are shown in **Figure 6**, where the short, medium, and long term diffusion rates are labeled and the values correspond to the parameters ε_s and ε_m in the **Table 3.** As we can see that theoretical mode can reproduce the entire MSD curve very well including intermediate time scale. For short-time super-diffusion, the slopes of the four sets of curves are all close to 2, specifically 1.974, 1.962, 2.227, and 1.937, which are consistent with the fitted values of ε_s. For medium-time super-diffusion, the slopes are also close to 2, specifically 1.996, 1.943, 1.992, and 1.992, again consistent with the fitted values of ε_m. In contrast, for long-time normal diffusion, the slopes all tend to approach 1.

4 Conclusions

In this paper, we constructed a large DFT dataset containing conformations related to both pure and SF_6/N_2 mixtures with different mixing ratios. Based on this dataset, constructed an accurate and efficient ML potential with DFT accuracy that can be used to describe the diffusion properties of SF_6/N_2 mixtures.

After obtaining the ML potential, we calculate the structural properties of SF_6 and N_2, and the results agree well with the DFT and experiment reference data. Then, we performed molecular dynamics simulations of SF_6 and N_2 dynamics in SF_6/N_2 mixtures based on the ML potential, we found that the motion of both SF_6 and N_2 exhibits the anomalous behavior. We systematically illustrate the anomalous characteristics of both SF_6 and N_2 motion. At short times, both SF_6 and N_2 performs super-diffusion through the ballistic motion. At intermediate times, a combination of the SF_6 molecular flexibility and cage effect result in the larger plateau value, while N_2 molecular showed no plateau stage. At longer times, both SF_6 and N_2 gradually turns to normal diffusion. A theoretical model is also offered to quantitatively describe this abnormal diffusion. This work gives a more completely physical understanding of SF_6 and N_2 dynamics in SF_6/N_2 mixtures, which provides important references for SF_6 /N_2 mixed electrical equipment leakage supplement.

5 Statements

Acknowledgments: Not applicable.

Funding Statement: This work is supported by the National Key Research and Development Program of China under Grant No. 2022YFB2 403700.

Author Contributions: The authors confirm contribution to the paper as follows: Conceptualization, methodology, visualization and writing—original draft preparation, Hanyan Xiao; Resources and visualization Tianxin Zhuang; Writing—original draft preparation, Jinggang Yang; Writing—review and editing, Ze Yin; Writing—review and editing, Zhaohui Zhang; Conceptualization, writing—original draft preparation, methodology, supervision and writing—review and editing, Ke Zhao. All authors reviewed the results and approved the final version of the manuscript.

Availability of Data and Materials: The data that support the findings of this study are available from the Corresponding Author, Ke Zhao, upon reasonable request.

Ethics Approval: Not applicable.

Conflicts of Interest: The author(s) declare(s) no conflicts of interest to report regarding the present study.

Reference

1. Christophorou, L. G.; Olthoff, J. K.; Green, D. S.; others. *Gases for Electrical Insulation and Arc Interruption: Possible Present and Future Alternatives to Pure SF6*; National Institute of Standards and Technology: Gaithersburg, 1997.
2. Christophorou, L. G.; Van Brunt, R. J. SF6/N2 Mixtures: Basic and HV Insulation Properties. *IEEE Transactions on Dielectrics and Electrical Insulation* **1995**, *2* (5), 952–1003.
3. Ding, R.; Zhao, K.; Xiao, H.; Chen, S.; Li, Y.; Ke, K. Effect of O2 on Insulation Performance and Decomposition Characteristic of C4F7N/N2Gas Mixture at High Gas Pressure. *High Voltage Apparatus*, 2021, *57*, 129–138.
4. Chen, H.; Li, D.; Yu, L.; Yang, H.; Tian, Y.; Yuan, S.; Liu, D. Theoretical Study on Diffusion Characteristics of SF6and N2Mixed Gases Based on Molecular Dynamics. *Industrial Safety and Environmental Protection* **2019**, *45* (12), 33–35.
5. Xiao, H.; Zhang, X. Studies on SF6 Degradation by Atmospheric Dielectric Barrier Discharge Plasma and Its Combination

with Catalysts. Doctor's Degree, 2018. https://kns.cnki.net/kcms2/article/abstract?v=X0pQrW14MIvt7SA04D4wMS_FgbUA34AMWB0bj7yX02Th0RlsT1pCO88dqwnonLo7Ew7CmsfwPJbkeZBGd5mcYQeQ56lh1X2nZe9uJwemGCbGtGbmiwnbXi7UKfGTrJYPsQGpDR6X-Hr0pKEzhXWPx56xFDBDJMzow0LmJp paU1tQDHU5ViR_sTFpyu8s8q6gbURMeiDVKM=&uniplatform=NZKPT&language=CHS.

6. Du, S.; Zhang, J. Molecular Simulation of Properties Change of Epoxy Resin for Insulator of DC GIL. Bachelor's Degree, 10.27623/d.cnki.gzkyu.2021.001319, 2021. https://link.cnki.net/doi/10.27623/d.cnki.gzkyu.2021.001319.
7. Poling, B. E.; Prausnitz, J. M.; O'connell, J. P.; others. *The Properties of Gases and Liquids*; Mcgraw-hill New York, 2001; Vol. 5.
8. Perry, C. E.; others. Handbook. *Chemical Engineers "Handbook", Third Edition, l950, Pages 39l and lO9-llO* **1963**.
9. Kestin, J.; Khalifa, H. E.; Ro, S. T.; Wakeham, W. A. The Viscosity and Diffusion Coefficients of Eighteen Binary Gaseous Systems. *Physica A: Statistical Mechanics and its Applications* **1977**, *88* (2), 242–260. https://doi.org/10.1016/0378-4371(77)90003-6.
10. Haghighi, B.; Djavanmardi, A. H.; Papari, M. M.; Najafi, M. Prediction of the Transport Properties of SF 6 with O 2, CO 2, CF 4, N 2 and CH 4 Mixtures at Low Density by the Inversion Method (Part II). *Journal of Theoretical and Computational Chemistry* **2004**, *3* (01), 69–90.
11. Olivet, A.; Vega, L. F. Predictions of Transport Properties in Gaseous Mixtures of Sulfur Hexafluoride and Nitrogen. *J. Phys. Chem. C* **2007**, *111* (43), 16013–16020. https://doi.org/10.1021/jp0743222.
12. Olivet, A.; Duque, D.; Vega, L. F. Sulfur Hexafluoride's Liquid-Vapor Coexistence Curve, Interfacial Properties, and Diffusion Coefficients as Predicted by a Simple Rigid Model. *The Journal of chemical physics* **2005**, *123* (19).
13. Olivet, A.; Duque, D.; Vega, L. F. Analysis of Electron Interactions in Dielectric Gases. *Journal of Applied Physics* **2007**, *101* (2).
14. Olivet, A.; Vega, L. F. Optimized Molecular Force Field for Sulfur Hexafluoride Simulations. *The Journal of chemical physics* **2007**, *126* (14).
15. Jolly, D. L.; and Bearman, R. J. Molecular Dynamics Simulation of the Mutual and Self Diffusion Coefficients in Lennard-Jones Liquid Mixtures. *Molecular Physics* **1980**, *41* (1), 137–147. https://doi.org/10.1080/00268978000102631.
16. Schoen, M.; and Hoheisel, C. The Mutual Diffusion Coefficient D 12 in Binary Liquid Model Mixtures. Molecular Dynamics Calculations Based on Lennard-Jones (12-6) Potentials: I. The Method of Determination. *Molecular Physics* **1984**, *52* (1), 33–56. https://doi.org/10.1080/00268978400101041.
17. Stoker, J. M.; Rowley, R. L. Molecular Dynamics Simulation of Real-Fluid Mutual Diffusion Coefficients with the Lennard-Jones Potential Model. *The Journal of chemical physics* **1989**, *91* (6), 3670–3676.
18. Zhou, Y.; Miller, G. H. Mutual Diffusion in Binary Ar-Kr Mixtures and Empirical Diffusion Models. *Phys. Rev. E* **1996**, *53* (2), 1587–1601. https://doi.org/10.1103/PhysRevE.53.1587.
19. Fernández, G. A.; Vrabec, J.; Hasse, H. A Molecular Simulation Study of Shear and Bulk Viscosity and Thermal Conductivity of Simple Real Fluids. *Fluid Phase Equilibria* **2004**,*221*(1),157–163. https://doi.org/10.1016/j.fluid.2004.05.011.
20. Fernández, G. A.; Vrabec, J.; Hasse, H. Self-Diffusion and Binary Maxwell–Stefan Diffusion Coefficients of Quadrupolar Real Fluids from Molecular Simulation. *Int J Thermophys* **2005**, *26* (5), 1389–1407. https://doi.org/10.1007/s10765-005-8093-6.
21. Van De Ven-Lucassen, I. M.; THIJS, J. V. A. J. V.; DER ZANDEN, P. J. K. Using Molecular Dynamics to Obtain Maxwell-Stefan Diffusion Coefficients in Liquid Systems. *Molecular Physics* **1998**, *94* (3), 495–503. https://doi.org/10.1080/002689798168006.
22. Dysthe, D. K.; Fuchs, A. H.; Rousseau, B. Prediction of Fluid Mixture Transport Properties by Molecular Dynamics. *International Journal of Thermophysics* **1998**, *19* (2), 437–448. https://doi.org/10.1023/A:1022513411043.
23. Rivera, J. L.; Alejandre, J. Transport Properties of Nitrogen and N-Alkane Binary Mixtures. *Fluid phase equilibria* **2001**, *185* (1–2), 389–396.

24. Zhou, Z.; Todd, B. D.; Travis, K. P.; Sadus, R. J. A Molecular Dynamics Study of Nitric Oxide in Water: Diffusion and Structure. *J Chem Phys* **2005**, *123* (5), 054505. https://doi.org/10.1063/1.1992482.
25. Zhang, C.; Yang, X. Molecular Dynamics Simulation of Ethanol/Water Mixtures for Structure and Diffusion Properties. *Fluid Phase Equilibria* **2005**, *231* (1), 1–10. https://doi.org/10.1016/j.fluid.2005.03.018.
26. Zhang, L.; Wang, Q.; Liu, Y.-C.; Zhang, L.-Z. On the Mutual Diffusion Properties of Ethanol-Water Mixtures. *The Journal of chemical physics* **2006**, *125* (10).
27. Zhang, L.; Han, J.; Wang, H.; Car, R.; E, W. Deep Potential Molecular Dynamics: A Scalable Model with the Accuracy of Quantum Mechanics. *Phys. Rev. Lett.* **2018**, *1 20* (14),143001. https://doi.org/10.1103/ Phys RevLett.120.143001.
28. Butler, K. T.; Davies, D. W.; Cartwright, H.; Isayev, O.; Walsh, A. Machine Learning for Molecular and Materials Science. *Nature* **2018**, *559* (7715), 547–555. https://doi.org/10. 1038/s41586-018-0337-2.
29. Unke, O. T.; Chmiela, S.; Sauceda, H. E.; Gastegger, M.; Poltavsky, I.; Schütt, K. T.; Tkatchenko, A.; Müller, K.-R. Machine Learning Force Fields. *Chem. Rev.* **2021**, *121* (16),10142–10186. https://doi.org/10.1021/ac s.chemrev.0c01111.
30. Bartók, A. P.; Payne, M. C.; Kondor, R.; Csányi, G. Gaussian Approximation Potentials: The Accuracy of Quantum Mechanics, without the Electrons. *Phys. Rev. Lett.* **2010**, *104* (13), 136403. https://doi.org/ 10.1103/PhysRevLett.104.136403.
31. Behler, J.; Parrinello, M. Generalized Neural-Network Representation of High-Dimensional Potential-Energy Surfaces. *Phys. Rev. Lett.* **2007**, *98* (14), 146401. https://doi.org/10.110 3/PhysRevLett.98.146401.
32. Artrith, N.; Behler, J. High-Dimensional Neural Network Potentials for Metal Surfaces: A Prototype Study for Copper. *Phys. Rev. B* **2012**,*85* (4),045439. https://doi.org/10.1103/ Phys RevB.85.045439.
33. Xia, Y.; Sautet, P. Plasma Oxidation of Copper: Molecular Dynamics Study with Neural Network Potentials. *ACS Nano* **2022**, *16* (12), 20680–20692. https://doi.org/10. 102 1/acsnano.2c07712.
34. Zhao, J.; Byggmästar, J.; He, H.; Nordlund, K.; Djurabekova, F.; Hua, M. Complex Ga2O3 Polymorphs Explored by Accurate and General-Purpose Machine-Learning Interatomic Potentials. *npj Comput Mater* **20 23**, *9* (1), 1–10. https://doi.org/10.1038/s4 15 24-023-01117-1.
35. Bartók, A. P.; Kermode, J.; Bernstein, N.; Csányi, G. Machine Learning a General-Purpose Interatomic Potential for Silicon. *Phys. Rev. X* **2018**, *8* (4), 041048. https://doi. org/10.1103/PhysRevX.8.041048.
36. Behler, J.; Martoňák, R.; Donadio, D.; Parrinello, M. Pressure-induced Phase Transitions in Silicon Studied by Neural Network-based Metadynamics Simulations. *Physica Status Solidi (b)* **2008**,*245*(12), 26 18–2629. https://doi.org/10.1002/pssb.200844219.
37. Li, H.; Meng, X.; Jing, Y.; Cong, L.; Zhang, X.; Zhao, J.; Sun, Y.; Li, W.; Yan, J.; Yang, J.; Li, X. Primary Radiation Damage in Si1−xGex Alloys: Molecular Dynamics Study with Machine-Learning Interatomic Potential. *Computational Materials Science* **2025**, *246*, 113484. https://doi.org/10.1016/j.commatsci. 2024.113484.
38. Li, H.; Jing, Y.; Liu, Z.; Cong, L.; Zhao, J.; Sun, Y.; Li, W.; Yan, J.; Yang, J.; Li, X. A Machine-Learning Interatomic Potential to Study Dry/Wet Oxidation Process of Silicon. *Journal of Applied Physics* **2024**, *136* (9), 095302. https://doi.org/10.1063/5.0219764.
39. Niu, H.; Jing, Y.; Sun, Y.; Guo, L.; Aluru, N. R.; Li, W.; Yang, J.; Li, X. On the Anomalous Diffusion of Proton in Y-Doped BaZrO3 Perovskite Oxide. *Solid State Ionics* **2022**, *376*, 115859. https://doi.org/10.1016/j.ssi.20 22.115859.
40. Niu, H.; Yang, Y.; Jensen, S.; Holzmann, M.; Pierleoni, C.; Ceperley, D. M. Stable Solid Molecular Hydrogen above 900 K from a Machine-Learned Potential Trained with Diffusion Quantum Monte Carlo. *Phys. Rev. Lett.* **2023**, *130* (7), 076102. https://doi.org/10. 1103/PhysRevLett.130.076102.
41. Niu, H.; Zhao, J.; Li, H.; Sun, Y.; Park, J. H.; Jing, Y.; Li, W.; Yang, J.; Li, X. A Machine-Learning Interatomic Potential to Understand Primary Radiation Damage of Silicon. *Computational Materials Science* **2023**, *218*, 111970. https://doi.org/10.1016/j.commatsci. 2022.111970.

42. Hamedani, A.; Byggmästar ,J.; Djurabekova ,F.; Alahyarizadeh ,G.; Ghaderi ,R.; Minuchehr ,A.; and Nordlund, K. Insights into the Primary Radiation Damage of Silicon by a Machine Learning Interatomic Potential. *Materials Research Letters* **2020**, *8* (10), 364–372. https://doi.org/10.1080/21663831.2020.1771451.
43. Kresse, G.; Furthmüller, J. Efficiency of Ab-Initio Total Energy Calculations for Metals and Semiconductors Using a Plane-Wave Basis Set. *Computational materials science* **1996**, *6* (1), 15–50.
44. Kresse, G.; Joubert, D. From Ultrasoft Pseudopotentials to the Projector Augmented-Wave Method. *Physical review b* **1999**, *59* (3), 1758.
45. Kresse, G.; Furthmüller, J. Efficient Iterative Schemes for *Ab Initio* Total-Energy Calculations Using a Plane-Wave Basis Set. *Phys. Rev. B* **1996**, *54* (16), 11169–11186. https://doi.org/10.1103/PhysRevB.54.11169.
46. Perdew, J. P.; Burke, K.; Ernzerhof, M. Generalized Gradient Approximation Made Simple. *Phys. Rev. Lett.* **1996**, *77* (18), 3865–3868. https://doi.org/10.1103/PhysRevLett.77.3865.
47. Behler, J. Constructing High-dimensional Neural Network Potentials: A Tutorial Review. *Int J of Quantum Chemistry* **2015**, *115*(16), 1032–1050. https://doi.org/10.1002/qua.24890.
48. Metzler, R.; Jeon, J.-H.; G. Cherstvy, A.; Barkai, E. Anomalous Diffusion Models and Their Properties: Non-Stationarity, Non-Ergodicity, and Ageing at the Centenary of Single Particle Tracking. *Physical Chemistry Chemical Physics* **2014**, *16* (44), 24128–24164. https://doi.org/10.1039/C4CP03465A.
49. Shin, J.; Cherstvy, A. G.; Metzler, R. Self-Subdiffusion in Solutions of Star-Shaped Crowders: Non-Monotonic Effects of Inter-Particle Interactions. *New J. Phys.* **2015**, *17* (11), 113028. https://doi.org/10.1088/1367-2630/17/11/113028.
50. Nosé, S. A Unified Formulation of the Constant Temperature Molecular Dynamics Methods. *The Journal of chemical physics* **1984**, *81* (1), 511–519. https://doi.org/10.1063/1.447334.
51. Hoover, W. G. Canonical Dynamics: Equilibrium Phase-Space Distributions. *Phys. Rev. A* **1985**,*31*(3),1695–1697. https://doi.org/10.1103/PhysRevA.31.1695.
52. Suzuki, T. The Determination of the Diffusion Rate of SF6 into Nitrogen. *IEEE Transactions on Electrical Insulation* **1982**, *EI-17* (1), 34–38. https://doi.org/10.1109/TEI.1982.298567.
53. Mburu, C. W.; Gaita, S. M.; Knee, C. S.; Gatari, M. J.; Karlsson, M. Influence of Yttrium Concentration on Local Structure in BaZr1–xYxO3−δ Based Proton Conductors. *J. Phys. Chem. C* **2017**, *121* (30), 16174–16181. https://doi.org/10.1021/acs.jpcc.7b05023.
54. Bjørheim, T. S.; Kotomin, E. A.; Maier, J. Hydration Entropy of BaZrO3 from First Principles Phonon Calculations. *J. Mater. Chem. A* **2015**, *3* (14), 7639–7648. https://doi.org/10.1039/C4TA06880G.
55. Edmond, K. V.; Elsesser, M. T.; Hunter, G. L.; Pine, D. J.; Weeks, E. R. Decoupling of Rotational and Translational Diffusion in Supercooled Colloidal Fluids. *Proceedings of the National Academy of Sciences* **2012**, *109* (44),17891–17896. https://doi.org/10.1073/pnas.1203328109.
56. Richard, R. M.; Abbott, B. J. Versatile Elastic-Plastic Stress-Strain Formula. *Journal of the Engineering Mechanics Division* **1975**, *101* (4), 511–515. https://doi.org/10.1061/ JMCEA3.0002047.